Thermal Emission Spectroscopy of Single, Isolated Carbon Nanoparticles: Effects of Particle Size, Material, Charge, Excitation Wavelength, and Thermal History

*Bryan A. Long, Daniel J. Rodriguez‡, Chris Y. Lau‡, Madeline Schultz, and Scott L. Anderson**

Chemistry Department, University of Utah, 315 S. 1400 E., Salt Lake City, UT 84112

‡*Equal contributions*

**Corresponding author: anderson@chem.utah.edu*

Supporting Information

Optical System Design:

Figure S1 shows the NPMS optics design. The trap is shown near the center of the dashed rectangle representing the vacuum chamber, and mirrors for focusing the CO_2 laser through the trap are shown, along with the laser beam path. 532 nm or other lasers are focused through the trap into the plane of the figure. The insertable thermocouple (TC) calibration emitter is shown schematically above the trap, and the coordinate system used in the following description is shown above that.

Light emitted axially (in the +z direction) from the trap center is collected by a five element lens system consisting of a 35 mm focal length achromatic doublet, a 100 mm focal length achromatic

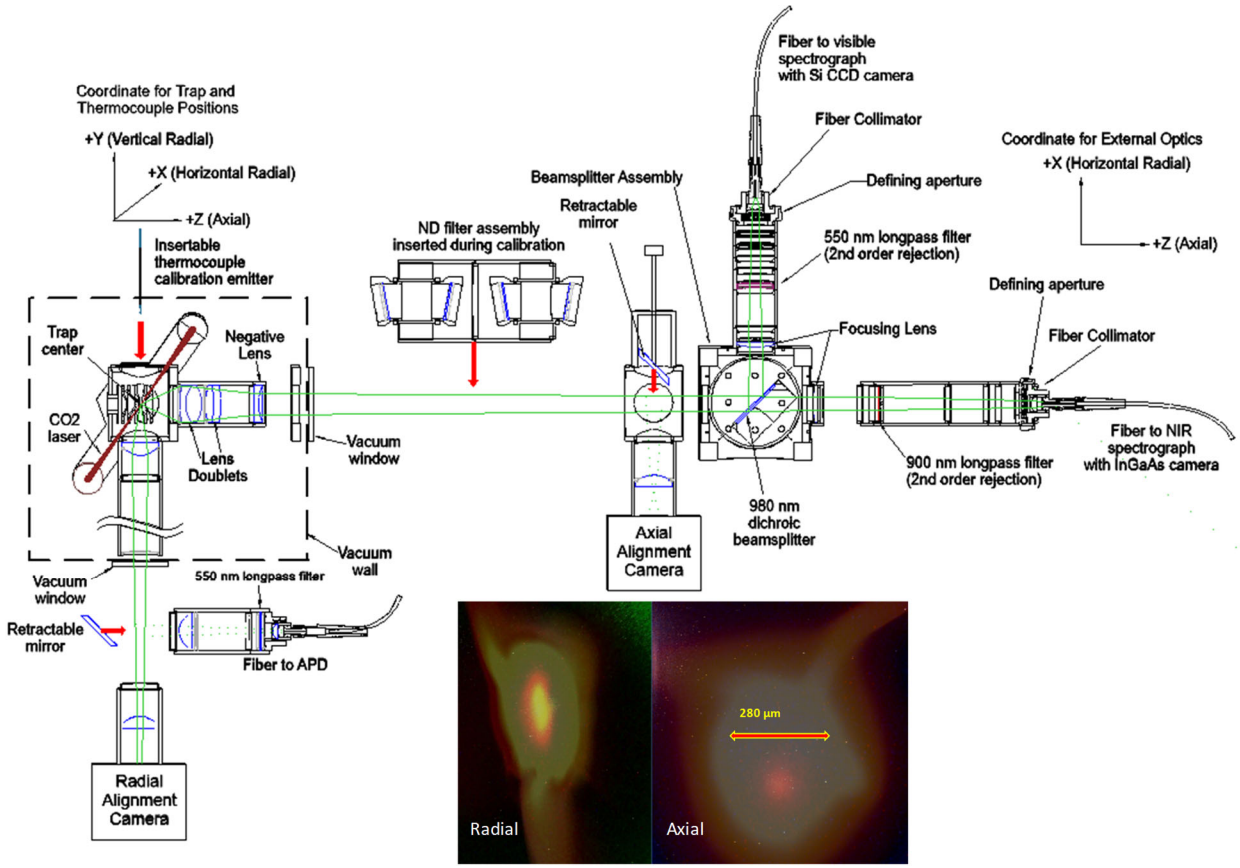

Figure S1. Alignment camera images at the bottom show views of a single NP (bright red/yellow spots) superimposed on images of the TC (larger irregular grey/green features), positioned for calibration experiments. Thermal emission is collected out of the bottom of the trap for mass and charge determination, and along the trap axis for spectra/T_{NP} measurements.

doublet, and a -75 mm focal length lens. This collects about one steradian solid angle from the trap center, and forms it into a slightly convergent beam. When the TC is used in calibration experiments, the ND filter assembly is inserted, cutting the light intensity by a factor of ~10^8, with transmission vs. wavelength measured as described previously.[1] For alignment purposes, a mirror can be inserted into the beam path, directing the light onto a room temperature CCD camera (The Imaging Source) that captures magnified images of the trap center from the axial direction for

alignment purposes. During spectral measurements, the mirror is retracted, allowing the light to reach a 980 nm dichroic beamsplitter that reflects wavelengths (λ) < 980 nm ("visible") and passes light with λ > 980 ("nIR"). The visible beam is passed through a 100 mm focal length plano-convex lens, a 550 nm long pass filter used to block scattered 532 nm laser light, and then is injected into a 1 mm diameter low OH optical fiber using a fiber collimator (Thorlabs, f = 8.00 mm, NA = 0.50, F240SMA-780 nm). The visible spectrum is dispersed by an Andor Shamrock 163 spectrograph equipped with silver-coated mirrors and grating, and measured by a back-illuminated Si CCD camera with 2000 pixel x 256 pixel CCD array with pixel sizes 15 μm x 15 μm, thermoelectrically cooled to -65 °C (Andor, DU416A-LDC-DD).

The nIR beam passes through a 175 mm focal length plano-convex lens, and a 900 nm long pass filter used to block 2nd order light in the nIR spectrum. A fiber collimator (Thorlabs, f = 8.12 mm, NA = 0.49, F240SMA-C-1310 nm) is used to inject the light into a 1 mm diameter low OH fiber, which conveys it to another Andor Shamrock 163 spectrograph, equipped with silver coated mirrors and grating. The nIR spectra are acquired by an InGaAs photodiode array camera, with a 512 pixel x 1 pixel array with pixels that are 25 μm wide by 500 μm high, cooled to -85° C (Andor, DU490A-1.7).

Light emitted radially out of the bottom of the trap is collected by a 31 mm aspheric achromat, and formed into a slightly convergent beam. Normally this is reflected by a retractable mirror, passed through a 50 mm focal length achromatic lens doublet, and injected into a 400 μm diameter low OH fiber that conveys the light to an avalanche photodiode (APD) pulse counting module (Laser Components Count). The APD signal is monitored as a function of time to detect the secular motion of the NP in the trap, for mass determination. When the mirror is retracted, the light is

focused onto a second room temperature CCD camera (The Imaging Source), generating a magnified view of the central volume of the trap from the radial direction, for alignment purposes.

Optical system calibration:

The optical system has non-idealities such as chromatic aberrations, detector quantum efficiencies, grating efficiencies, etc., that affect its sensitivity vs. wavelength, $S(\lambda)$, thus distorting the measured spectra. Before fitting spectra to extract temperatures, it is essential to correct the NP spectral intensities, i.e., we need to know $S(\lambda)$ quantitatively. To measure $S(\lambda)$ we need a calibration light source with well-known intensity vs. λ, small enough to fit into the trap center so that calibration can be done on the system as a whole, under conditions identical to those used for the NP spectral measurements.

As a calibration emitter, we use a micro-thermocouple (TC) with a roughly disk-shaped bead about 280 μm in diameter, and ~150 μm thick. The TC is positioned so that its bead is in the trap center, where it can be heated by the CO_2 laser, with the bead temperature read out electrically. The TC wire manufacturer (Concept Alloys) states that the accuracy in the temperature range of interest here is ±1% of the measurement in °C. To enable the TC bead to be positioned precisely and repeatedly, the TC is mounted on a precision XYZ vacuum manipulator, and the axial and radial alignment cameras allow the position in two orthogonal planes to be imaged. The approach to determining the correct TC position is to first trap a single NP, and image it with the two cameras, thus defining the trap center precisely. Then the TC is moved into the trap, heated, and its position is adjusted until it is at the position defined by the NP.

The bottom of Figure S1 shows superimposed images of a single NP and the TC, from the radial (left) and axial (right) alignment cameras. In the radial camera image, looking from the bottom of the trap, the NP appears as a bright yellow/red oblong in the center, and the laser-heated TC

appears as the larger irregular pale green shape with lead wires visible extending from the bead at the top and bottom of the image. The axial camera shows the NP as a circular red spot, and the TC bead as a roughly circular pale grey area, with lead wires visible at the top extending to either side.

The NP image makes an important point: The effective "size" of the trapped NP as a light emitter is determined by the amplitude of its secular motion in the trap, which depends on NP mass and charge and the trap operating conditions. For the hot carbon NPs of interest here, the NP effective size (FWHM) is typically in the 30 to 40 μm range along the axial direction, with double this "size" in the radial direction, hence the oblong appearance of the NP in the radial camera image. Thus, for light collection along the axis, the NP emitter "size" is ~60 - 80 μm in diameter.

Figure S2 illustrates the process of using the TC emission spectra to determine S(λ) and to correct NP spectra. Figure S2A shows a typical TC spectrum measured at a junction temperature of 2316 K. This measurement was done with the ND filter assembly inserted into the optical path, so that the intensity of the calibration spectrum was similar to those for single NPs. The scale is in counts/second/m^2 of TC emitter surface area (area ≈ 2.93x10-8 m^2). The approach to measuring the ND filter assembly transmission has been described previously, along with the transmission vs. wavelength.[1] Figure S2B shows the predicted TC emission spectrum, which is the product of three functions: 1. The Planck's law emission function for an ideal blackbody at 2316 K. 2. The emissivity of the W-Re TC at 2316 K[2-5] 3. The ND filter assembly transmission. The ratio of Figure S2A to Figure S2B is the desired S(λ) function, which is plotted in Figure S2C. Figure S2D shows a typical raw single NP spectrum, measured for a single graphite NP of mass 14.93 MDa. Figure S2E shows the result of dividing Figure S2D by Figure S2C, to obtain a sensitivity-corrected NP spectrum.

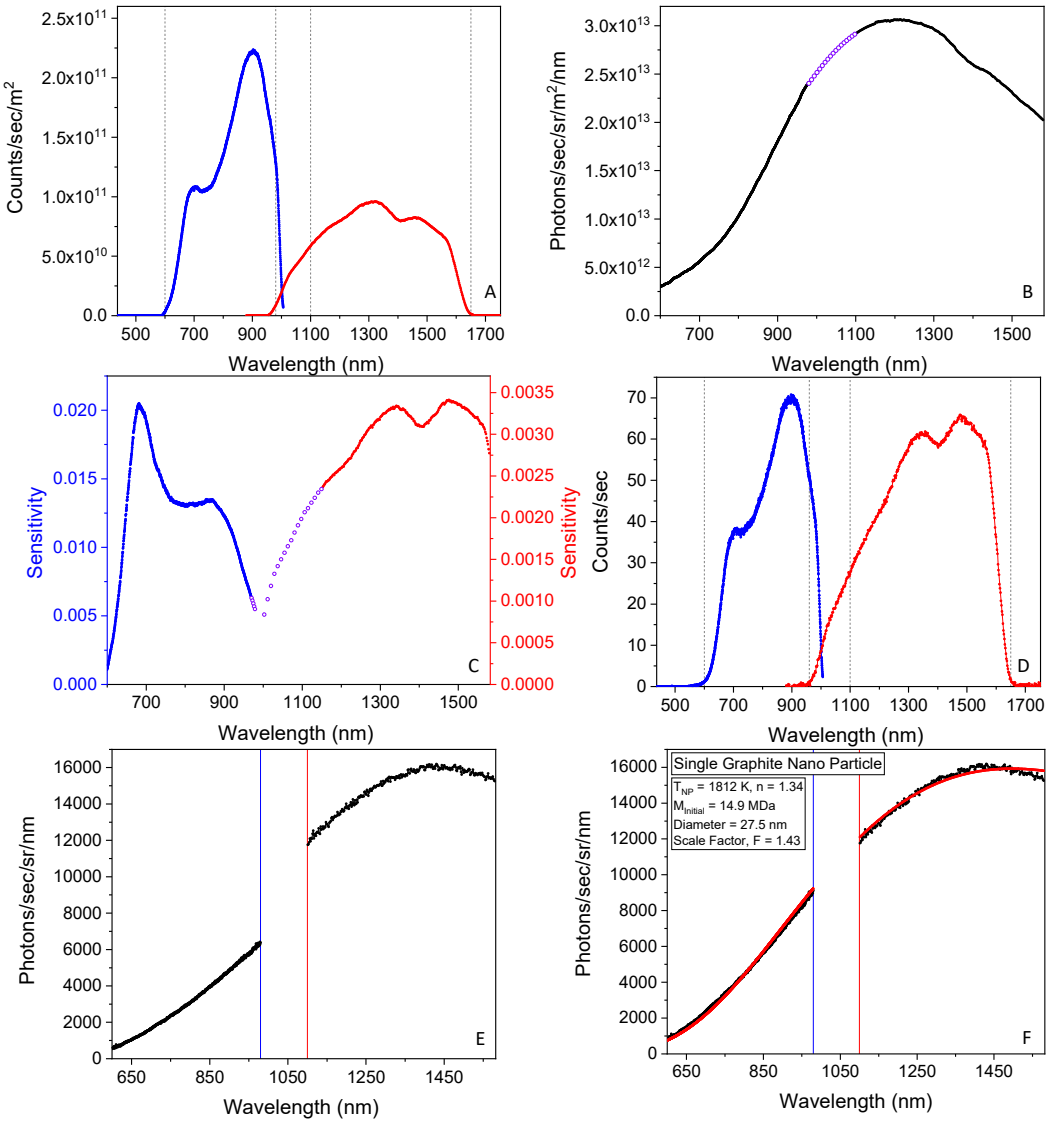

Figure S2. Data illustrating how the sensitivity function, S(λ), is extracted, and NP spectra are intensity corrected. Frame A is the raw spectrum for the TC heated to 2316 K. B is the theoretical spectrum, calculated as the product of Planck's law, the emissivity of the TC material, and the transmission of the ND filter assembly. C is the extracted S(λ) function, *i.e.* the ratio of A to B. D is a typical single raw NP spectrum. E shows the corrected NP spectrum, showing intensity mismatch between the visible and nIR. F is the final corrected spectrum with fit, after applying the visible scale factor.

Note that there is a spectral region from 980 to 1100 nm where both the visible and nIR spectrographs have low sensitivity because of the combined effects of the dichroic beamsplitter, the CCD quantum efficiency, and the grating efficiency of the nIR spectrograph. As a result, the signal in this "gap" region is low, and uncertainty is high. In the fitting process described below for T_{NP} determination, this gap region is given zero weight.

Figure S2E shows one final step in the NP spectral correction process. Note that the visible and nIR spectra do not match up across the spectral gap region, i.e., the corrected visible intensity is slightly too low to match smoothly to the nIR data. This effect is believed to be a result of the fact that our visible camera uses a 2D array that is 3.84 mm tall, whereas the 1D nIR camera array is only 500 μm tall, (but equipped with a cylindrical lens to help reduce the height of the dispersed light on the array). Because the TC (~280 μm) is significantly larger than the ~80 μm effective radial emitter size for typical NPs, the solid angle of light injected into the fibers (numerical aperture 0.5) is higher for the TC than for NPs, resulting in a somewhat larger solid angle entering the spectrographs. The taller visible array captures more of this "extra" light than the nIR array, and as a result, the visible portion of $S(\lambda)$ is larger than it should be for correcting spectra from the smaller NP emitters. Thus, the intensity of the visible portion of the corrected NP spectra tends to be slightly too small to match up smoothly to the nIR section. This hypothesis is supported by the observation that changing the effective NP emitter size by varying the trapping conditions, results in changes in the relative intensities of the visible and nIR spectra.

Therefore, it is necessary to scale the visible spectrum to ensure smooth matching to the nIR spectrum across the gap. The approach used is to fit the data just on either side of the gap (900 to 950 nm in the visible and 1030 to 1200 nm in the nIR), to a smooth function, with the visible spectrum scale factor as one of the fit parameters. As a smooth function, we use Planck's law

times a power law model for the NP emissivity ($\epsilon \propto \lambda^{-n}$), *i.e.*, the same function used to fit spectra for T_{NP} determination, but with n fixed at 1.4. The n parameter affects the curvature of the fitting function, but because only a narrow λ range is fit to extract the visible spectrum scale factor, the scale factor is not very dependent on the exponent. 1.4 was chosen as being typical for carbon NPs, and the correct value for room temperature graphite (see Figure S3). Figure S2F shows the result of applying the scale factor to the visible spectrum. The visible spectrum scale factor varies slightly from NP to NP, and in this case, it was 1.34. The effects of systematically varying this scale factor on temperatures extracted from spectral fitting are explored below.

Power law approximation to the scattering theory emissivity function:

The NP spectra are fit to a function that is the product of Planck's law times and emissivity function, ϵ(λ). As noted in the manuscript, scattering theory predicts that in the limit of NPs much smaller than the wavelengths emitted, as is the case here, $\epsilon(\lambda) = \frac{8\pi r}{\lambda} Im\left(\frac{(n+ik)^2-1}{(n+ik)^2+2}\right)$, where n and k are the real and imaginary components of the index of refraction of the material at the wavelengths and temperature of interest.[6] Figure S3 shows ϵ(λ) for graphite, calculated from the scattering theory expression, using room temperature n and k values from the literature.[7] The figure also shows the best power law fit to the scattering theory result: $\epsilon(\lambda) \propto \lambda^{-n}$, n = 1.41. The maximum difference between the two curves

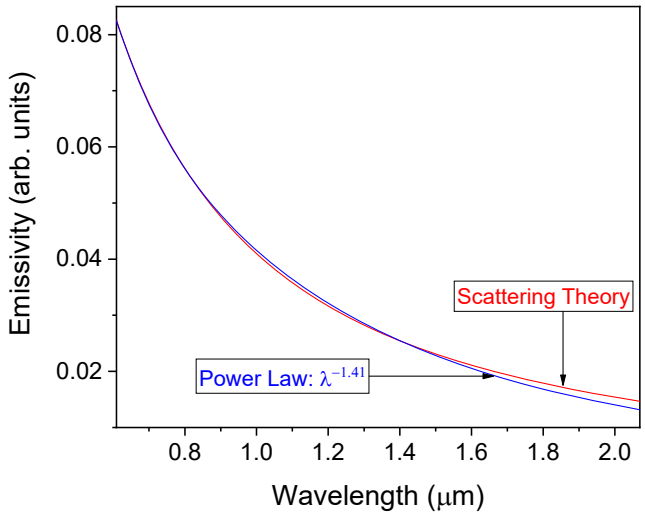

Figure S3. Comparison of the calculated emissivity function based on small particle scattering theory (Red) using room temperature graphite n and k data, to a power law model, λ^{-n} (Blue).

in the wavelength range we measure is ~3%. Ideally we would use the correct $\epsilon(\lambda)$ function in fitting NP spectra, however, the necessary index of refraction (or equivalent dielectric) parameters are not available for the materials of interest, at high temperatures, over the wavelength range of interest. More fundamentally, bulk optical properties would be inaccurate for NPs, due to the large number of surface and defect states in NPs. Therefore, we are forced to adopt a model $\epsilon(\lambda)$ function, and the power law model at least has the virtue of having roughly the correct shape and introducing a minimum number of adjustable parameters.

Sensitivity of extracted T_{NP} values to the position of the TC, and to TC temperature used in calibration:

Figures S4A-C, show the effects of moving the TC calibration emitter to different positions in the trap, *i.e.*, deliberately positioning it so that it is not at the trap center. Each figure shows traces of NP temperature (T_{NP}) vs. time from an experiment in which a single NP was heated using a 532 nm laser, with its temperature stepped from ~1200 K to ~2000 K, then dropped to ~1400 K. The 532 nm laser was not being stabilized during this test, and its intensity fluctuated significantly, driving fluctuations in T_{NP}. All the traces shown in Figures S4A-C are based on the same raw NP emission spectra, but corrected using TC calibration spectra obtained with the TC emitter at the trap center (black trace), and deliberately misaligned by ± 0.05 and ± 0.1 mm in the X, Y, and Z directions, relative to trap center. The important point is how much the T_{NP} traces obtained at different TC emitter positions vary, *i.e.*, how sensitive the T_{NP} calibration is to mis-aligning the TC emitter relative to trap center. The TC temperature, T_{TC}, during these experiments was kept close to 2300 K, and measured electrically in conjunction with each spectral measurement.

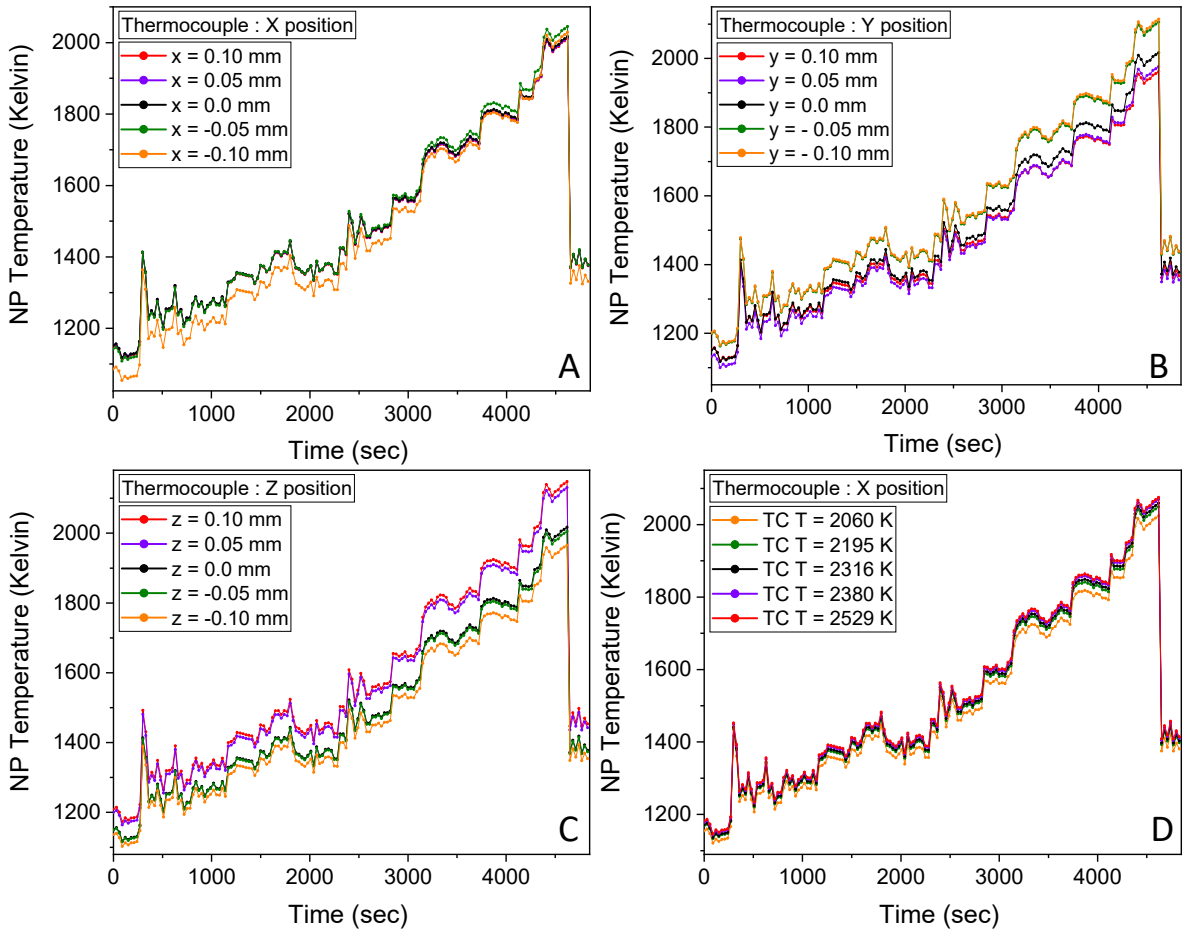

Figure S4. Temperature profile as a function of time for a single NP being heated at different laser powers. Figures A-C are correcting the same single NP raw emission spectra with different thermocouple emission spectra as a function of thermocouple position in the ion trap. Figure D is correcting the same single NP raw emission spectra but with the thermocouple in the optimal position of the trap but at different temperatures.

In Figure S4A, the TC was moved radially in the x direction, as defined in Figure S1, while keeping the y and z coordinates centered on the trap. This corresponds to horizontal motion of the right hand TC image shown in Figure S1. It can be seen that if the TC is positioned at x= -0.10 mm with respect to the trap center the T_{NP} values extracted for the NP are shifted significantly to lower temperatures, particularly for low T_{NP} values. For example, the shift is roughly -60 K for

T_{NP} near 1200 K, but only –30K for T_{NP} above 1500 K, and only -10 K at temperatures greater than 1800 K. For misalignments of -0.05 mm and for both +0.05 and +0.10 mm, the variations in T_{NP} relative to the values extracted for the TC at the trap center are much smaller – averaging roughly ± 6 K over the entire T_{NP} range.

Figure S4B gives analogous data for deliberate misalignment of the TC emitter in the y direction, where +y corresponds to moving the right-hand TC image in Figure S1 up, and –y is downward motion. Here the effects of misalignment, particularly of having the TC positioned too high in the trap, are larger. For y = -0.1 mm and -0.05 mm, T_{NP} values are similar, and shifted by ~-50 K at low T_{NP} and by ~-90 K at high T_{NP}, relative to the T_{NP} values obtained at y = 0.0. For positive y misalignments (y = 0.05 and 0.1 mm) the shifts are also similar to each other, but much smaller, remaining within 20 K of the values measured for y = 0.0 at all T_{NP}. The larger shifts observed for negative y misalignments are attributed to the effect of collecting light emitted from the wires leading to the TC bead. These wires connect to the bead at its top, and are significantly cooler than the laser-heated bead. Thus, for TC displacements to –y, the optical system picks up more light from the lead wires, which would tend to give TC spectra colder than the bead temperature, and therefore cause the calibrated T_{NP} higher, as is observed. Knowing this, we position the TC so that the lower part of the bead is at the trap center, as shown in the left image in Figure S1.

Figure S4C shows the effects of moving the TC axially in the trap, with +z corresponding to moving closer to the collection lens. The TC positions z = 0.05 mm (purple trace, T_{TC} = 2303 K) and z = 0.1 mm (red trace, T_{TC} = 2302 K) cause ~+100 K shifts in the T_{NP} values obtained from the TC spectra. In contrast, moving the TC to z = -0.05 mm, *i.e.*, slightly further from the collection lens, had no significant effect, and moving to z = -0.1 mm caused shifts to lower T_{NP} ranging from ~-20 K at low T_{NP} to ~-50 K. The larger effects from shifting the TC closer to the collection lens

makes sense – the NP is a diffuse emitter extending axially ~± 0.03 mm relative to the trap center, whereas the TC emitter is the surface of the TC bead facing the collection lens. Thus, as shown in the left image in Figure S1, when z = 0, the TC surface is actually ~ 0.06 mm closer to the lens than the trap center. Thus for small negative displacements of the TC, its front surface actually moves closer to the trap center, *i.e.* to the average NP position. For positive displacements, however, the TC surface is shifted increasingly farther from the average position of the NP, hence introducing significant chromatic effects on the TC spectra that affect the T_{NP} calibration. Knowing this, we are careful to position the TC with its center at, or slightly behind the trap center.

Given the ~25 μm precision with which the TC can be positioned in the X, Y, and Z directions, and the results in Figures S4A-C, we estimate that the aggregate effects of TC misalignment on the extracted T_{NP} values range from ~ ±3.2% at low end of our T_{NP} range, to ±3.5% at high T_{NP} values.

In principle, the TC temperature used to generate the sensitivity calibration needed to correct the NP spectra should not matter, however this assumes that there is no error in reading the TC temperature (T_{TC}) and in calculating the emissivity used to correct the TC spectra. To test for possible T_{TC} effects, Figure S4D shows the effects of correcting the same NP data using TC spectra measured at different TC temperatures, with the TC positioned at x = y = z = 0. There are effects of T_{TC} on the extracted T_{NP} values, but they are small, as expected. For all but the lowest T_{TC} value (2060 K), the variations in T_{NP} are less than 10 K at low T_{NP}, and less than 16 K for high T_{NP}, corresponding to ≤ 0.8% uncertainty in T_{NP}. Using the 2060 K TC data introduces larger errors (~19 K at low T_{NP}, 35 K at high T_{NP}), probably because the emitter is too cold to give good intensities at short wavelengths. Obviously, we avoid use of low TC temperatures in correcting

NP spectra, thus the uncertainty in T_{NP} values due to this TC temperature effect is estimated to be ≤0.8%.

Effects of optical system misalignment on measured and corrected NP spectra, and on the T_{NP} values extracted by fitting:

Figures S5 – S9 show the effects on raw TC and NP spectra and corrected NP spectra (and extracted T_{NP} values) of deliberately misaligning various optical components. Note that misalignment generally results in substantial decreases in signal intensities,

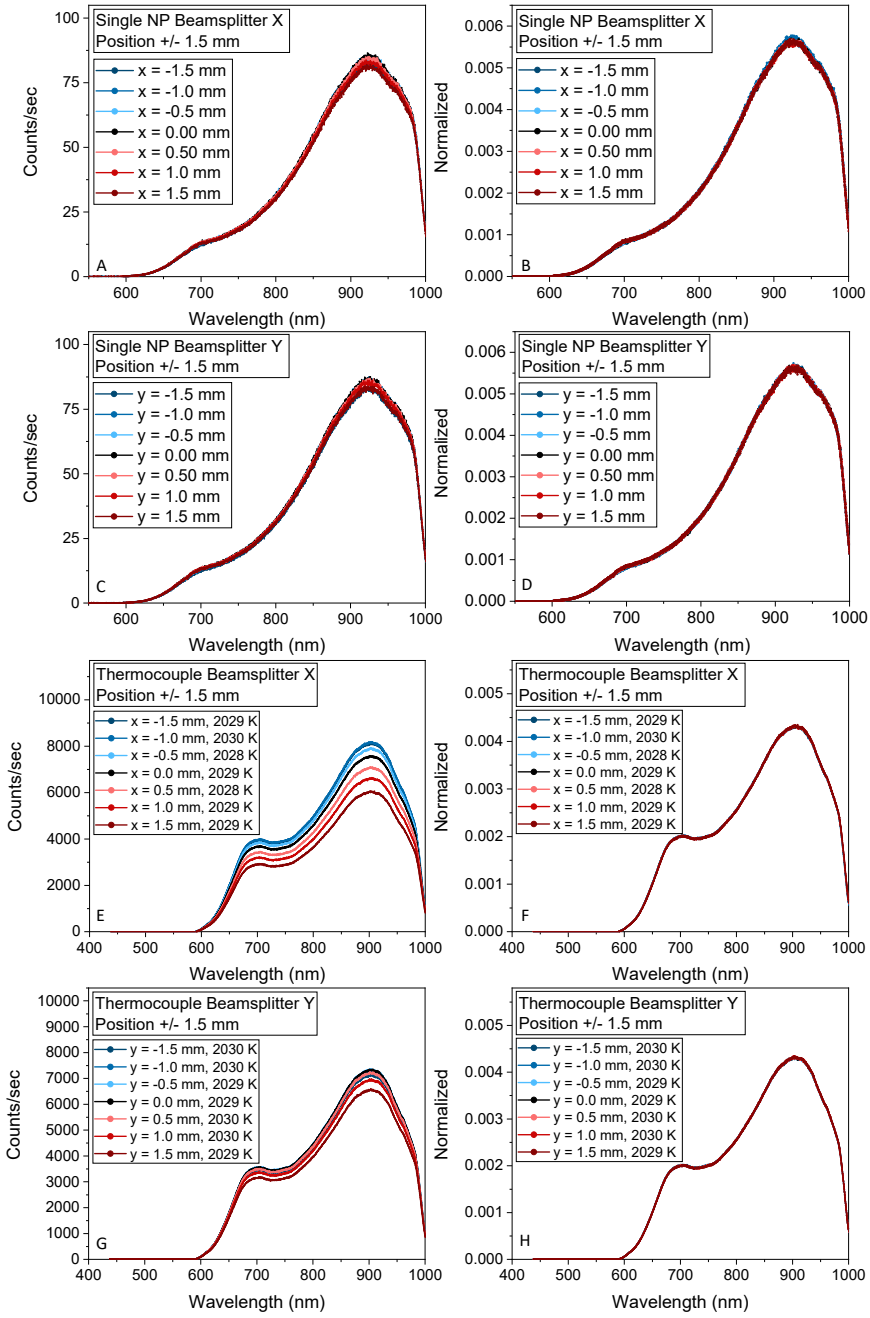

Figure S5. Raw NP visible emission spectra (A-D) and TC visible emission spectra (E-H). A, C, E, and G show the effects on the emission spectra of varying the beamsplitter's x and y positions by +/- 1.5 mm. Figures B, D, F, and H show the normalized intensities to allow shape changes observed.

however, from the T_{NP} determination perspective, what is important are two factors: 1. How does the misalignment affect the *shape* of the spectra, as opposed to the intensity? To show changes in intensity and shape, we present both raw and normalized TC and NP spectra. 2. If there are changes in spectral shape from misalignments, are they the same for the TC and NP spectra? If so, they cancel in the calibration process. If not, they are apparent as changes in the corrected NP spectra.

In Figure S5 the raw visible emission spectra for a single NP and for the TC are shown as a function of displacements of the beamsplitter assembly in the x and y directions. Note that in making such comparisons, we kept the NP at relatively low T_{NP}, so that it did not sublime significantly on the experimental time scale, and we attempted to keep the temperature constant by holding the heating laser at constant intensity, using a PID program to stabilize the laser (unlike the measurements in Figure S4). As shown in Figure S1, beamsplitter assembly motion also moves the visible focusing lens and fiber collimator. The y motion does not move the visible beam path, therefore the lens and collimator become radially misaligned with respect to the beam. The x motion of the beamsplitter shifts the visible beam path, and again, the beam becomes radially misaligned with the lens and collimator.

The left side of Figure S5 shows raw spectra, and the right side shows the same spectra, normalized to allow changes in shape to be seen. In Figures S5A and S5E, the x position of the beamsplitter is changed by ±1.5 mm relative to the position that gives maximum intensity for the NP spectra, while measuring the NP and TC raw spectra. Figure S5C and S5G show analogous effects of ±1.5 mm misalignments in the y direction. It can be seen that radial misalignment of the focusing optics has significant effects on visible spectral intensity, but as shown in Figures S5B,

S5D, S5F, and S5H, the spectral shape, which is what is important in T_{NP} determination, is relatively insensitive to this kind of misalignment.

Note that motion of the beamsplitter assembly does not shift the transmitted nIR beam path, but because the 175 mm nIR focusing lens is attached to the assembly, its motion does misalign the lens with respect to the beam path, thereby deflecting the beam slightly such that it becomes radially misaligned with respect to the nIR collimator. The effect of this radial misalignment on the nIR spectra is similar to what is observed if the beamsplitter assembly is fixed, but the nIR collimator is translated to cause radial misalignment (Figures S6 and S7A-C). Because these effects are similar and quite small, a separate figure is not presented showing the effects on nIR spectra of x and y beamsplitter assembly motion. Similarly, small displacements of the beamsplitter assembly in the z direction have negligible effects on either visible or nIR spectra, and these data are not shown.

In Figures S6-S9, we explore the misalignment of the nIR fiber collimator, which is mounted separately, allowing x, y, and z motion with respect to the nIR beam path. This motion has no effect on the visible spectra. Figure S6 shows spectra for a single NP for nIR collimator positions misaligned by up to ± 0.4 mm in the x and y (*i.e.* radial) directions. Figure S6A and S6C show raw spectra and Figures S6B and S6D show the same spectra normalized so that shape differences can be seen. It can be seen that for x and y misalignment of the nIR collimator, there are significant intensity effects, but that the spectral shape is unaffected. Figures S7A-D show analogous TC

emission spectra, *i.e.*, raw and normalized spectra measured as a function of x and y misalignments up to ± 0.4 mm. Again, there is essentially no effect on the spectral shape. Figure S6E and S6F show how the integrated nIR signal from a single NP varies with x and y misalignment, showing that it is easy to find the optimum radial position for the collimator.

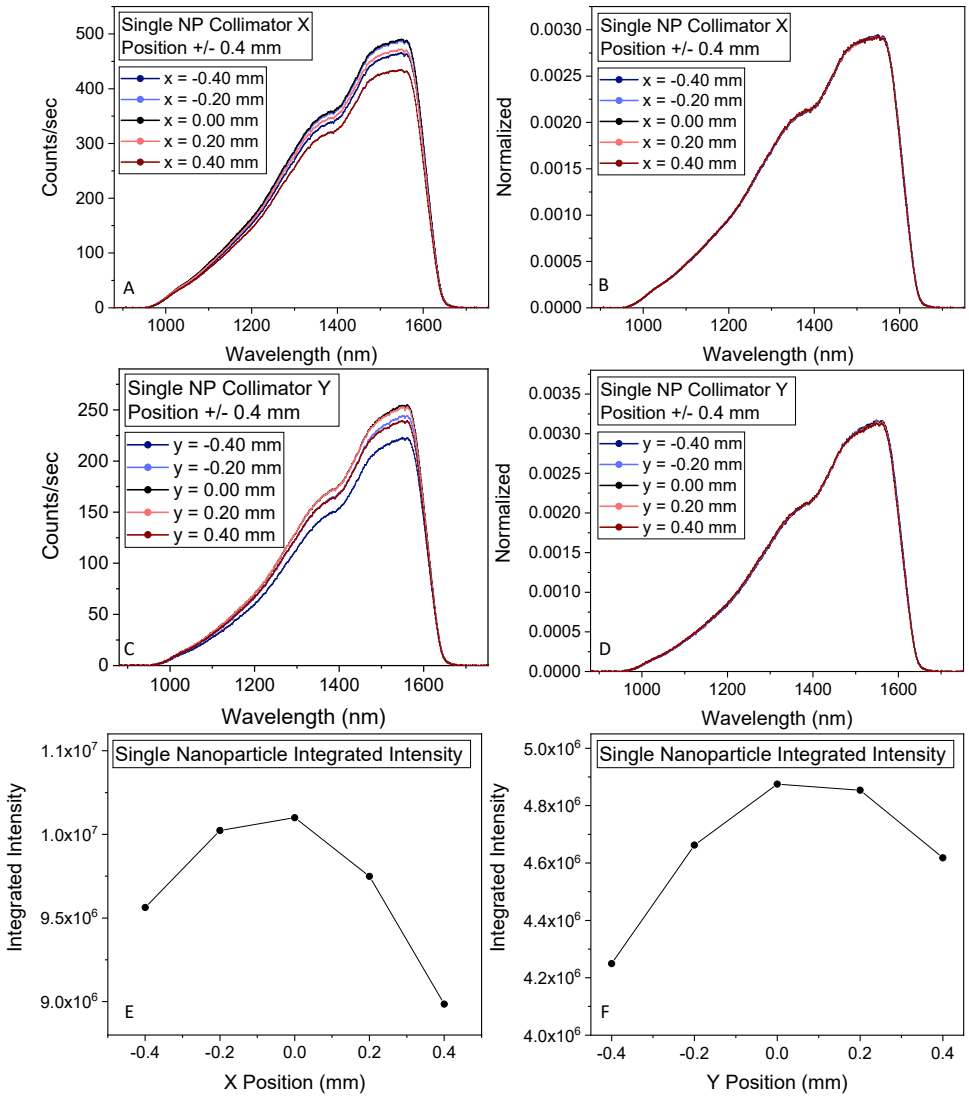

Figure S6. nIR emission spectra for a single carbon nanoparticle. Frames A and C show the effects of misalignment of the nIR fiber collimator on the raw intensities, and frames B and D show that the effects of nIR collimator on shape are negligible. Frames E and F simply show how the integrated spectral intensities vary with misalignment in the x and y directions.

The bottom half of Figure S7 shows the effects of nIR collimator x and y misalignment on the nIR part of the corrected NP spectra (there are not effects on the visible spectra). Figures S7E and S7G show that there are intensity changes in the corrected NP spectra as a function of collimator position, but Figure S7F and S7H show that the effects on spectral shape are small, as might be expected from small effects on the raw NP and TC spectral shapes. The T_{NP} values extracted by fitting these spectra (combined with visible

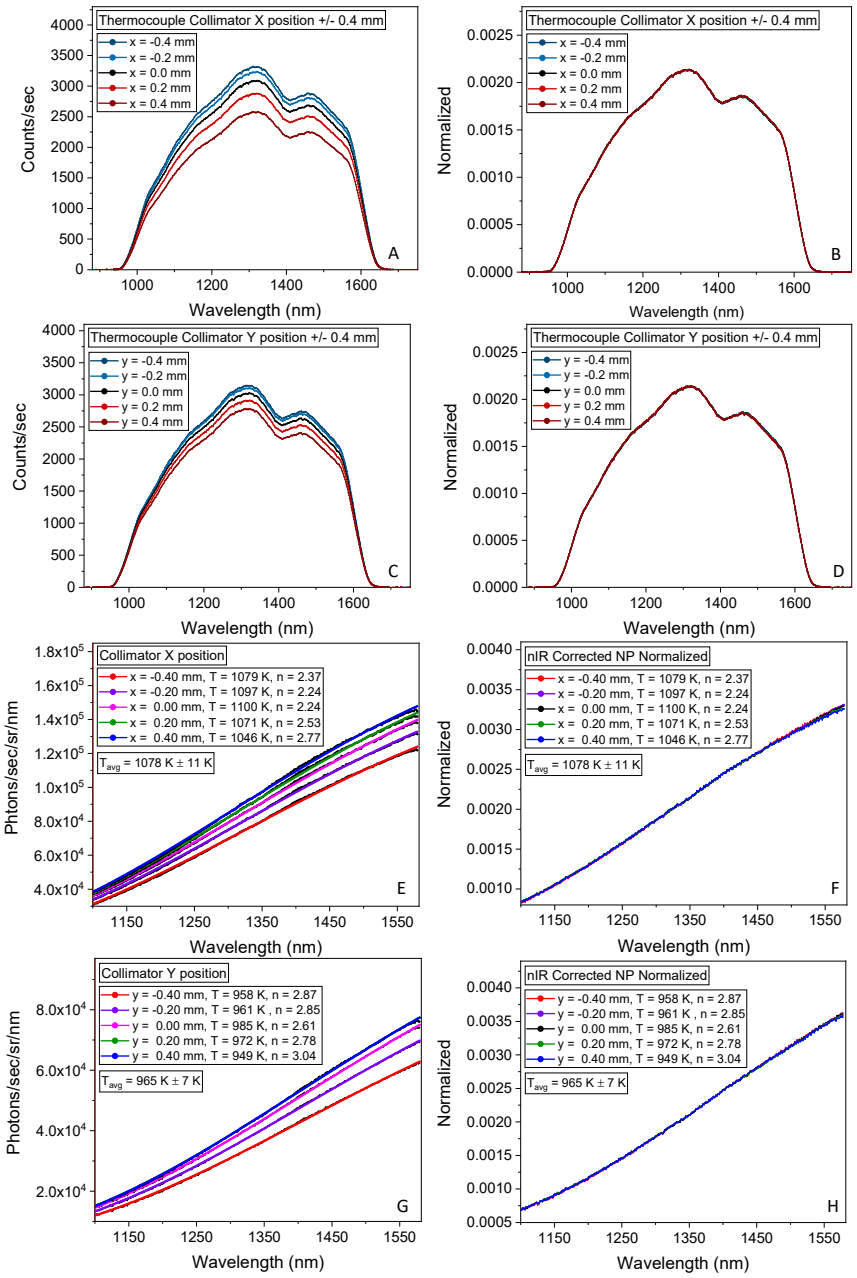

Figure S7. Frames A-D show raw TC nIR spectra at different X and Y collimator positions, taken at similar TC temperatures. Frames E and G are corrected NP spectra at different X and Y collimator positions, corrected using TC spectra taken at the same collimator positions. Images F and H are the spectra in E and G, normalized to show shape changes.

spectra taken at the same time) show ± 22 and ± 14 K variations (<±2%), however, it should be noted that the laser used to heat the NPs was not perfectly stable, thus it is almost certain that some of this T_{NP} variation was real, *i.e.*, not error due to collimator position.

Given the relatively sharp dependence of intensity on x and y position, which makes it straightforward to align it precisely,

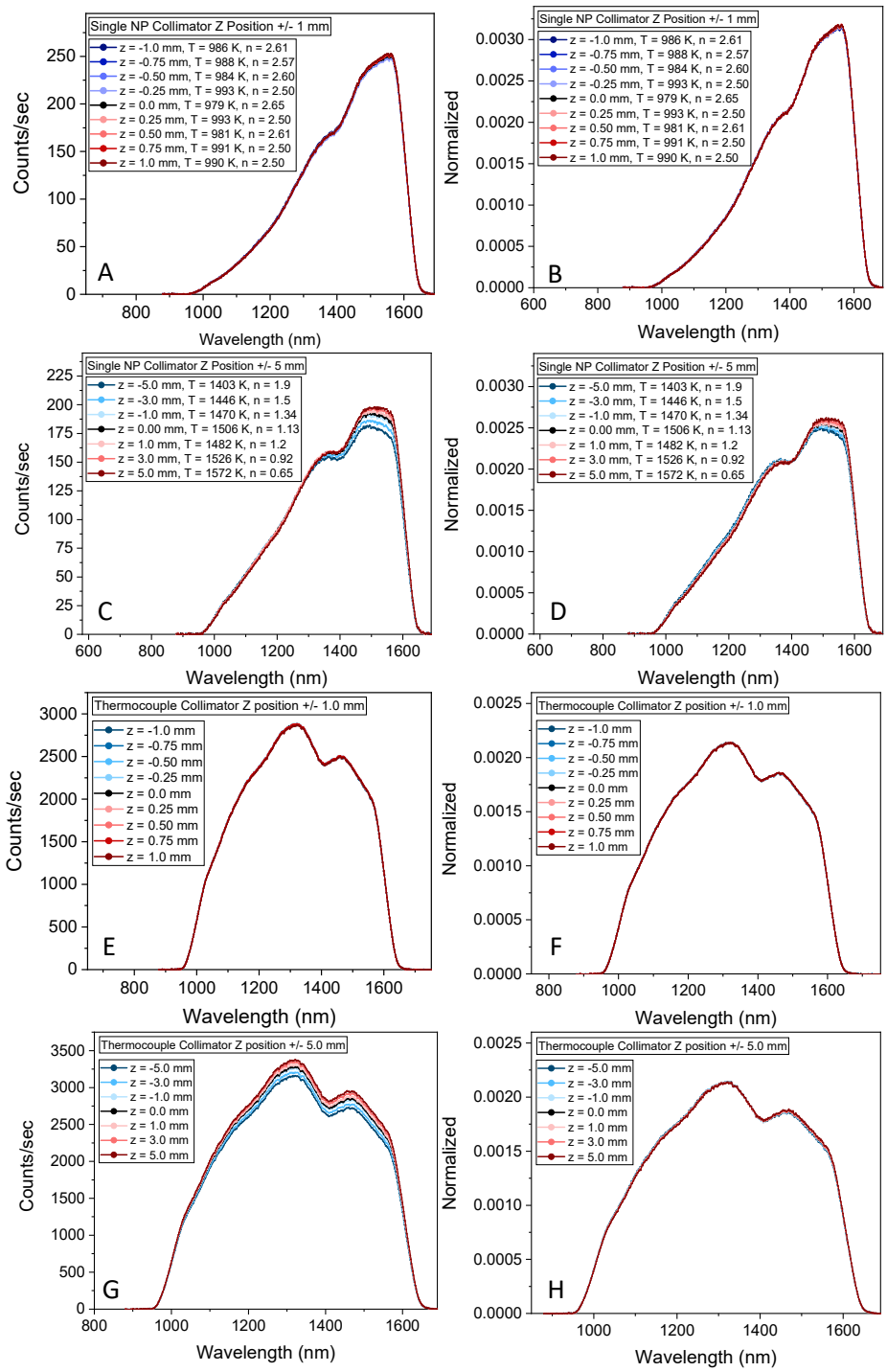

Figure S8. Frames A-D are raw nIR single NP emission spectra as a function of collimator Z position. Frames E-F are raw nIR TC emission spectra at the same Z positions. Frames A,B, E, and F shows small variations of collimator Z position (± 1.0 mm). Frames C, D, H, and G show effects of larger collimator misalignments up to ± 5.0 mm.

we conclude, that x and y collimator misalignment has negligible effect on the uncertainty of the T_{NP} measurements.

The positioning of the collimator in z (axial) direction is more problematic. Figures S8 and S9 show the effects of changing the z position of the nIR collimator, with all other optics left in their optimal positions. Figure S8 shows raw and normalized NP and TC spectra for z position changes of up to ±1 mm, relative to the optimal z position. Because long focal length lenses are used to couple the nIR light into the collimator, the intensity varies much more slowly with z than the x and y variations shown in Figure S6E and S6F, *i.e.*, it is not as straightforward to identify the optimal position. To find the optimal z position, the collimator was translated over a ± 11.5 mm range, measuring the fall off of intensity in both directions, and choosing the mid-point as the optimal z position. For collimator displacements up to ±1 mm (Figure S8A) the changes in raw NP spectra are small, and the normalized spectra (S8B) are essentially superimposable. Certainly any differences between spectra are well within the variation expected due to real variations in the NP temperature over the experiment time. For larger ±5 mm displacements of the collimator (S8C), there are larger changes in the spectral intensity, and after normalization (S8D), it can be seen that there are net shifts to the red or blue for large positive and negative z displacements, respectively. If the TC spectra had similar red and blue shifts, there would be no problem, however, as shown in the analogous TC spectra in Figures S8E-H, the TC spectra have smaller red and blue shifts. This difference reflects the larger size of the TC emitter (~280 μm) compared to the NP effective emitter size (~80 μm), which means that chromatic effects tend to average out more in the TC spectra than in those for the NPs.

The effects of z displacements on corrected NP spectra, and the T_{NP} values extracted by fitting them, are summarized in Figure S9. Note that for these experiments, relatively large NPs were

used to give good signal, while keeping T_{NP} low enough to minimize sublimation and other changes to the NP.

Figure S9A shows the corrected spectra for a single NP with $T_{NP} \approx 980$ K, also including the visible portion of the spectra because this is used in the fitting process.

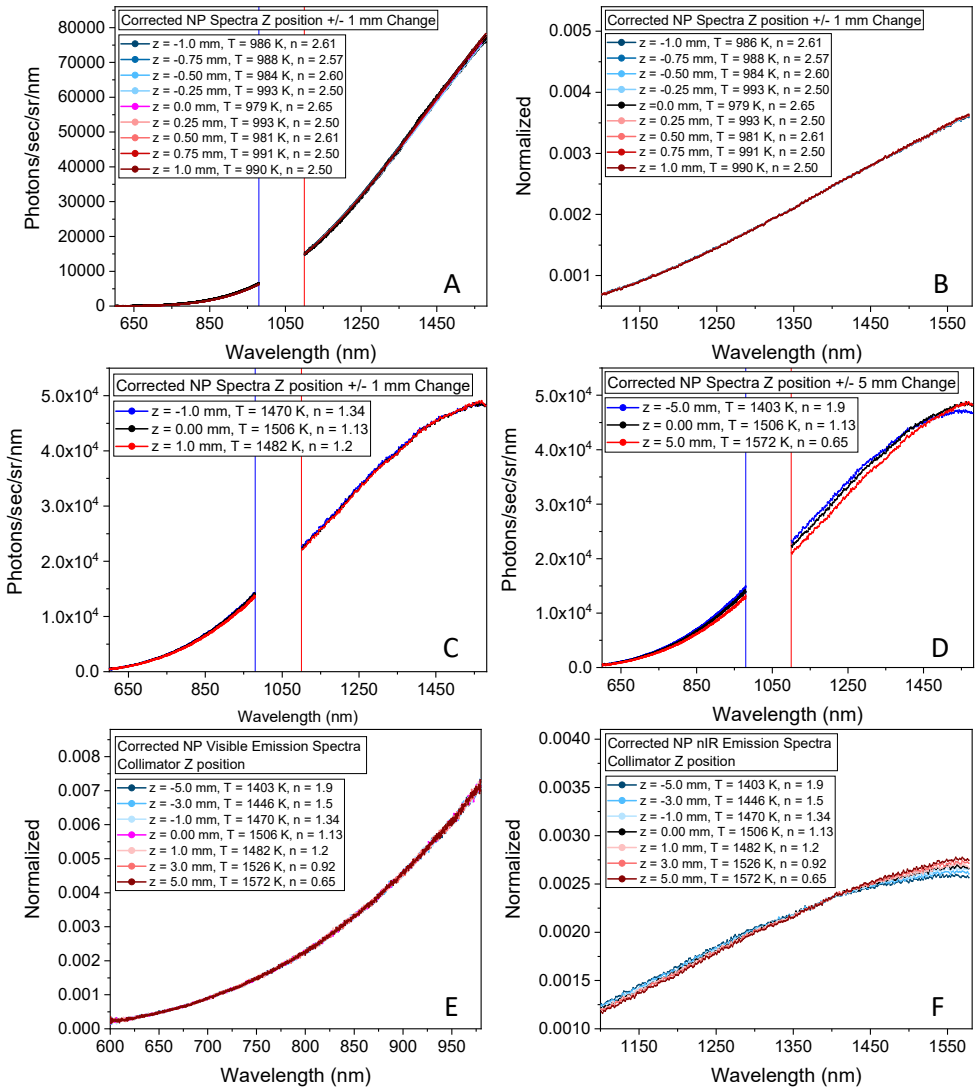

Figure S9. Corrected spectra for different NPs measured with different nIR collimator positions. A.) Effects of ± 1.0 mm changes in the Z position. B.) The nIR spectra, normalized to show shape changes. C.) Analogous unnormalized spectra for a different NP at higher T_{NP}. D.) Effects of ± 5 mm changes in the nIR collimator position. E.) Visible spectra showing that, as expected, moving the nIR collimator has no effect. F.) nIR spectra, normalized, as a function of± 5 mm misalignment of the nIR collimator.

For z displacements up to ±1 mm, T_{NP} varies by ≤ 14 K (≤ 1.4 %), however, T_{NP} fluctuates randomly rather than varying systematically with z. This is a sign that the T_{NP} fluctuations were not due to the z displacement, but rather reflect real T_{NP} variations due to laser intensity fluctuations. Figure S9B shows that the normalized nIR spectra are essentially superimposable. Figure S9C shows corrected spectra for a different NP at higher T_{NP}, also for ±1 mm z displacements. Again, T_{NP} varies randomly with z, by about 2% in this case. The fact that T_{NP} shows no systematic variation with z over this ±1 mm range is not surprising, given that the raw spectra (Figure S8B) are nearly superimposable.

Figure S9D shows the effects of ±5 mm z displacements – a range where significant, systematic red shifts were observed with increasing z in the spectra in Figure S8D. As expected, these spectral shifts result in systematic increases in the extracted T_{NP} values with increasing z. Figure S9E and S9F show the visible and nIR spectra from Figure S9D, normalized to allow shape changes to be observed. As expected, there are no changes in the visible spectral shapes, but the nIR region shows significant red shifting with increasing z.

Similar axial displacement measurements were done moving the visible collimator relative to the beamsplitter assembly by up to ±8 mm in the x direction, but no effects were observed on the shape of the visible part of the spectra. Indeed, the visible spectra are generally much less affected by misalignments of the optics or of the TC position, compared to the nIR spectra. In part, this probably reflects the fact that the achromatic doublets used in the collection system are optimized for the 750-1550 nm range, which is part of our "visible" spectrum. In addition, however, the 2D CCD array used to record the visible spectra is 3.84 mm tall, whereas the 1D InGaAs array used for the nIR spectra is only 0.5 mm tall. The nIR camera has a cylindrical lens to vertically compress the dispersed light onto the array, but some light still misses the array. As a result, the visible

detection efficiency is less sensitive to the divergence of light exiting the fiber, compared to that for the nIR spectrograph, and therefore, less sensitive to optical misalignments that affect how light couples into the fibers.

For x and y displacements of the nIR collimator, the intensity falls off rapidly – much faster than chromatic effects grow in. Therefore, the correct x and y positions are well defined, and we are able to position the collimator accurately enough that misalignment in these directions has a negligible effect on the uncertainty in T_{NP}. The same is not true for the z positioning, because the intensity maximum along this direction is much broader, and significant chromatic effects appear for ± z collimator displacements for which the intensity is only modestly affected. The method used to find the optimal z position for collimator is estimated to give the position to within ±0.5 mm, but for estimating the resulting effect on T_{NP} we assume that the position is uncertain by ±2 mm. From data analogous to that in Figure S9C-D, but for ±2 mm z motion of the collimator, we find that T_{NP} varied by a total of 86 K, corresponding to 5.6%. Therefore, we estimate this contribution to the uncertainty as ~±2.8 %.

Effects of varying the visible scale factor on fit quality and T_{NP}:

As discussed above, the intensity of the visible part of the spectrum must be scaled to match smoothly to the nIR part, and Figure S10 explores the effect of changing the scale factor, f, away from the best-fit value. In Figures S10A-C the spectrum is plotted with the best fit value of f (1.53) in blue, and the red and orange spectra show the effects of increasing or decreasing f by ±2%, ±5%, and ±10%. The two insets show more clearly how changing f affects both the visible spectra (the nIR is not scaled) and the resulting fits to the entire spectrum.

Consider the effect of changing f by ±10% (C). The visible inset shows how the change in scale factor shifts the spectra to increased or decreased intensity. Such a large change in f leads to gross

mismatching of the visible and nIR spectra, as can be seen by the resulting fits. Note that when f is increased by 10%, shifting the visible spectrum to higher intensity, the best fit is well below the experimental spectrum in the visible, and well above it in the nIR, *i.e.*, it essentially splits the differences between the now-mismatched visible and nIR spectra. Similarly, if the visible spectrum is scaled down by 10%, the fit is obviously too high in the visible. The same effect is clear when f is changed by ±5% (Figure S10B). Clearly such large variations in f can be excluded on basis of poor fitting.

On the other hand, when f is changed by only ±2% (Figure S10A), the fits now are within the scatter in the experimental spectra, *i.e.* the precision of the process used to determine the best-fit f value is ~±2%. (Note that to keep the spectral fits in the visible inset from overlapping, they have been offset, only for the ±2% case). If we take the variation in T_{NP} for the ±2% change in f as an estimate of this contribution to the

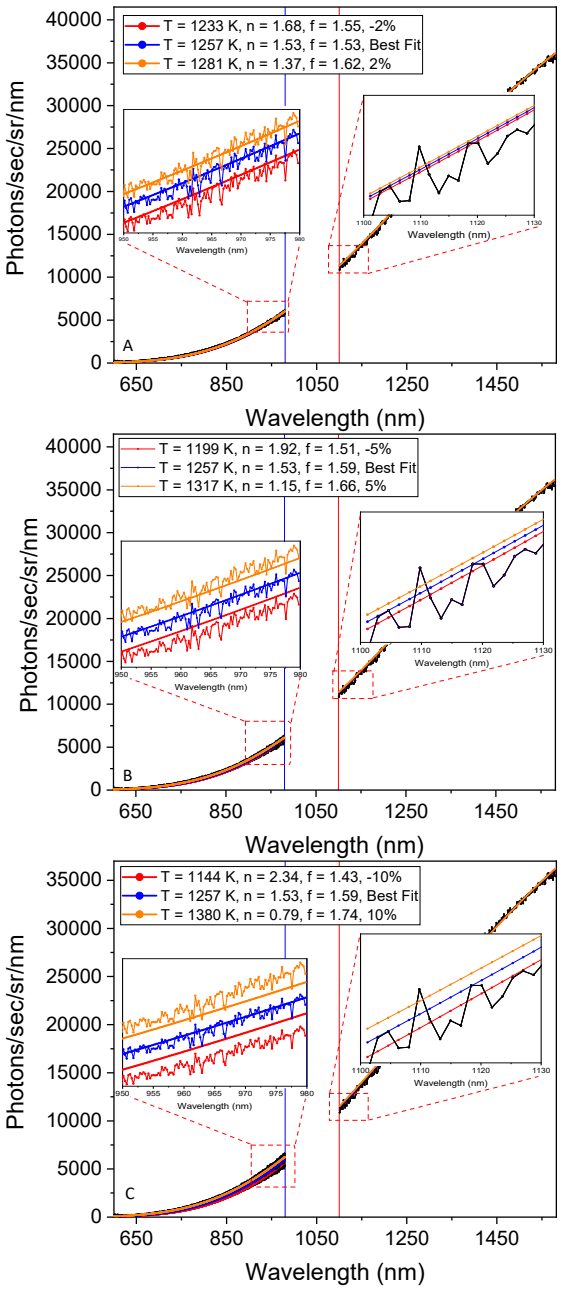

Figures S10. Images A-C show the effect of varying the best fit visible scale factor, f, by ±2%, ±5%, and ±10% from its best-fit value, determined as described above. Note that in the visible inset in A, the spectra and fits have been offset for clarity.

uncertainty in T_{NP}, the result is only ±24 K or ±1.9%.

Effects of spectral integration time:

To test for possible saturation effects in the visible and nIR cameras, Figure S11 shows spectra of a single graphite NP with M = 14.2 MDa, with the laser stabilized to have power, measured at the vacuum exit window, of 19.6 mW ± 0.28 mW. In Figure S11A, the spectra are plotted in terms of photons/sec/sr/nm of spectral bandwidth, and have been offset vertically so that the individual spectra can be seen clearly. In Figure S11B, the spectra are plotted without the offset so that their shapes can be compared.

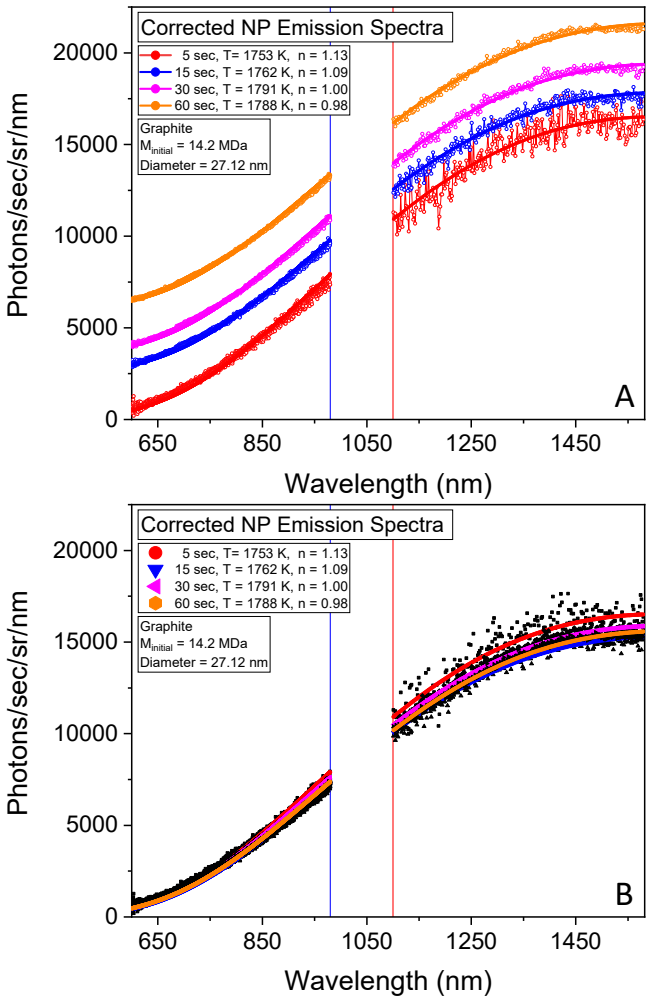

Figure S11. Emission spectra taken at different integration times of, 5, 15, 30, and 60 seconds for a single graphite NP with $M_{initial}$ = 14.2 MDa. In image A, the 15, 30, and 60 second integrations times are offset to show how the noise varies between spectra. Image B has no offset, and it showing that the overall intensity is similar between spectra.

As expected the short acquisition time spectra are relatively noisy, and the 5 second spectrum has slightly higher intensity. The 30 and 60 second spectra are essentially identical, and the T_{NP} and n values extracted from fitting them also have negligible differences. There may be a slight decrease in the apparent T_{NP} and increase in n

for the shorter time spectra, however, the variation in T_{NP} is certainly well within the fitting error for such noisy spectra.

Summary of the effects of optical system alignment and fitting on the uncertainties in T_{NP}.

As described above, the significant experimental contributions to uncertainties in the spectral shapes, hence T_{NP}, are: 1. Positioning of the TC during calibration (±3.2 to 3.5%), 2. The z position of the nIR collimator (±2.8 %), 3. The visible spectrum scale factor (± 1.9%). The positions of other optics are well enough defined and controlled that they do not contribute uncertainties of these magnitudes, and thus their contributions are considered negligible. Therefore, the total contribution to uncertainty in T_{NP} from these experimental issues is estimated to be ±4.8 %.

In addition, given typical signal/noise level in NP spectra, we estimate ~±4 % uncertainty in T_{NP} from fitting, assuming a fitting function consisting of Planck's law times the power law model for $\epsilon(\lambda)$. Therefore, the total estimated uncertainty in T_{NP} including both experimental and fitting uncertainties is ±6.2 %. As emphasized in the main paper, there is additional error associated with our choice of the power law function to model $\epsilon(\lambda)$, however, because the correct form of $\epsilon(\lambda)$ is unknown, it is not possible to estimate this error. We simply note that for many of the carbon materials, the fits to the NP spectra based on the power law $\epsilon(\lambda)$ model are quite good, suggesting that the error is relatively small.

Effects of varying n on extracted T_{NP} values:

One issue with using the power law model, however, is that the T_{NP} and n parameters both affect the curvature of the emission vs. λ, and while the effects are different, they are not orthogonal. Increasing the n parameter causes the fit function to fall off more rapidly at long wavelengths, and in fitting a spectrum, this fall off is compensated by decreasing T_{NP} in Planck's law, which increases the intensity at long wavelengths relative to short wavelengths. The result is a fitting function with more curvature, *i.e.*, higher at mid-wavelengths, and falling off more rapidly at both long and short wavelengths, compared to the function with best-fit n value. Conversely, decreasing n is compensated by increasing T_{NP}, which results in a fitting function with more gradual wavelength dependence.

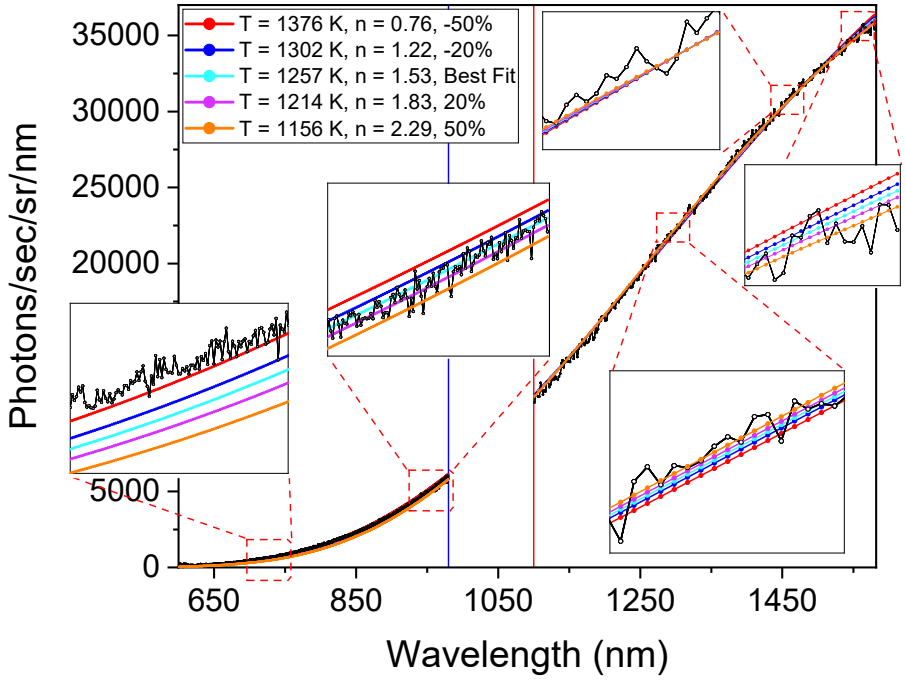

Figure S12. Effects of varying n, relative to its best fit value, on the fits and extracted T_{NP} values for a typical NP spectrum.

To illustrate this behavior, and estimate the resulting uncertainty in T_{NP}, Figure S12 shows how forcing the n parameter away from its best fit value affects the fit quality and extracted T_{NP} values.

The experimental spectrum being fit is for a carbon black NP of 85 MDa size, and the acquisition time was 30 seconds. The spectrum was first fit allowing n and T_{NP} (and the normalization constant) to vary, obtaining best fit values of T_{NP} = 1257 K, and n= 1.53. We then varied the n parameter by up to ±50%, refitting the spectrum allowing only T_{NP} (and the normalization) to vary. For clarity, the figure shows only the results for ±20% and ±50% variations, and to help show the effects more clearly, insets with magnified intensity scales are shown for five regions across the spectrum.

Because the power law model is only an approximation to the true emissivity function, even the best-fit function over- or under-shoots the experimental data in some spectral regions. Therefore, forcing n away from its best-fit value may improve the fit in some spectral regions, even though the overall fit is worsened. For example, using n = 2.29 improves the fit in the wavelength region near 1550 nm, however, such a high n value substantially worsens the fit over the entire range below 1000 nm. Similarly, using n = 0.76 gives the best fit in the region around 700 nm, but substantially worsens the fit for most of the rest of the spectrum. Similar effects are observed for the ±20% variations in n, but in that case, the deviations are on the same order as the estimated uncertainty in the relative spectral intensities (*i.e.*, spectral shape). The temperature variations associated with ±20% n variations are roughly $\pm$45 K (~±4%), and we take this as a rough estimate of the error associated with fitting any particular spectrum, *within the power law model*.

NP spectra for different materials compared, before and after >1900 K heating.

Figures S13 and S14 replot the spectra in figures 4A and for NP1 in Figure 5A and 5C and Figure 5D in the main text, to allow comparison between materials. In Figure S13, the volume-scaled intensities for NPs prior to >1900 K heating are shown on the left, and the post-heating spectra are

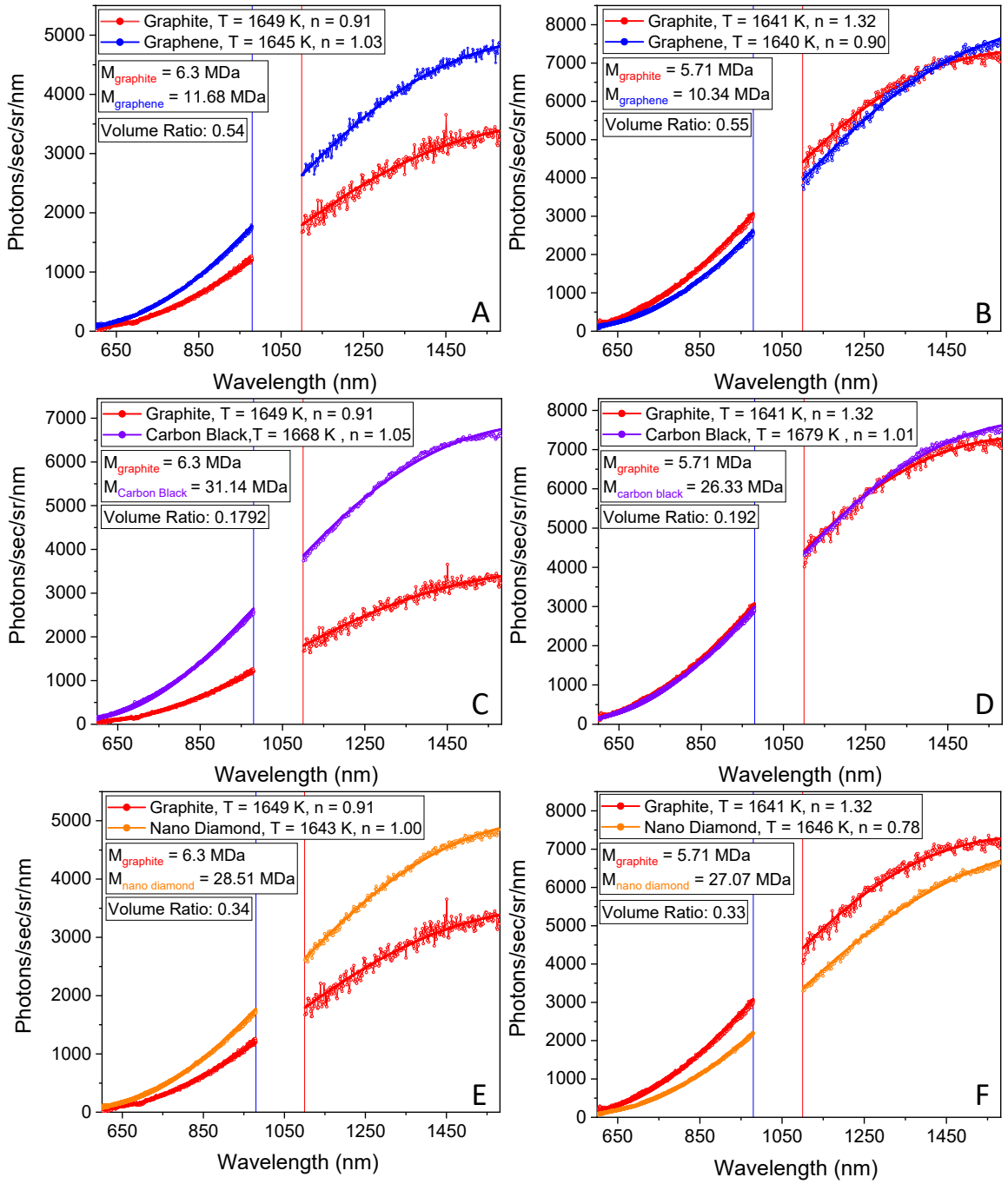

Figure S13. Emission spectra comparing the carbon NPs in figures 3 and 4, before and after heating. All spectra are volume scaled to allow direct comparison of intensities. The left column has spectra prior to heating above 1900 K. The right column shows spectra collected after >1900 K heating.

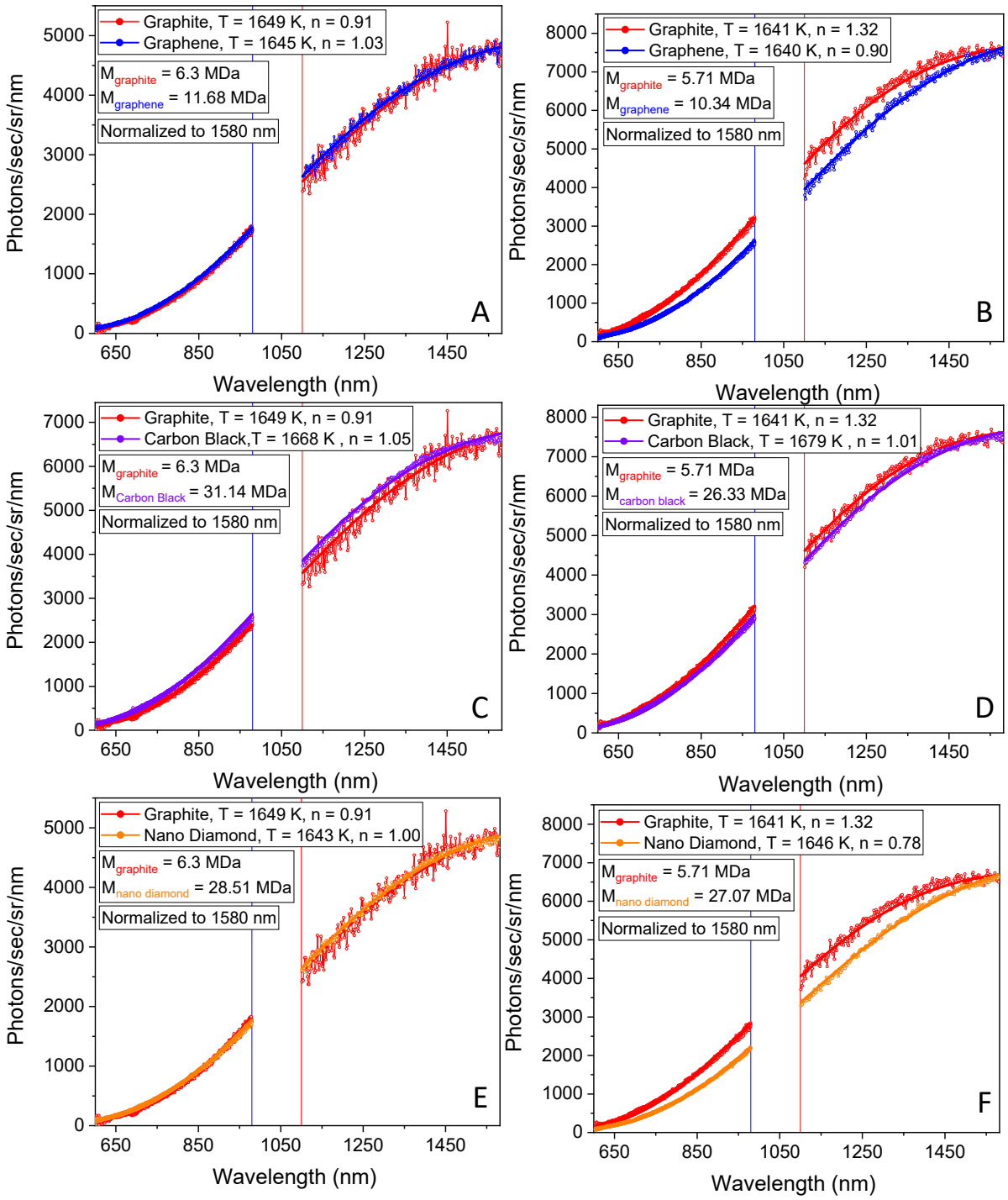

Figure S14. Emission spectra comparing the carbon NPs in figures 3 and 4, before and after heating. All spectra are normalized at 1580 nm to allow spectral shape comparison. The left column has spectra prior to heating above 1900 K. The right column shows spectra collected after >1900 K heating.

on the right. In Figure S14, the data are replotted, normalized at 1580 nm, to allow spectral shapes to be compared.

Effects of measuring T_{NP} while NP motion is being driven to measure the NP mass.

Figure S15 addresses the question of whether T_{NP} is significantly affected by the enhanced axial NP motion that occurs when the NP is being driven to measure mass, due to possible changes in chromatic effects as the NP position in the trap varies. In the figure, T_{NP} is shown vs. time for a single graphite NP with initial mass of 23.22 MDa as the NP was heated with 12.2 mW ±0.05 mW of 532 nm laser power, giving T_{NP} near 1500 K. The scatter in the T_{NP} values partly reflects signal/noise in the spectra, taken at relatively low T_{NP} to minimize sublimation, but in addition, the normal T_{NP} stabilization program was not being used.

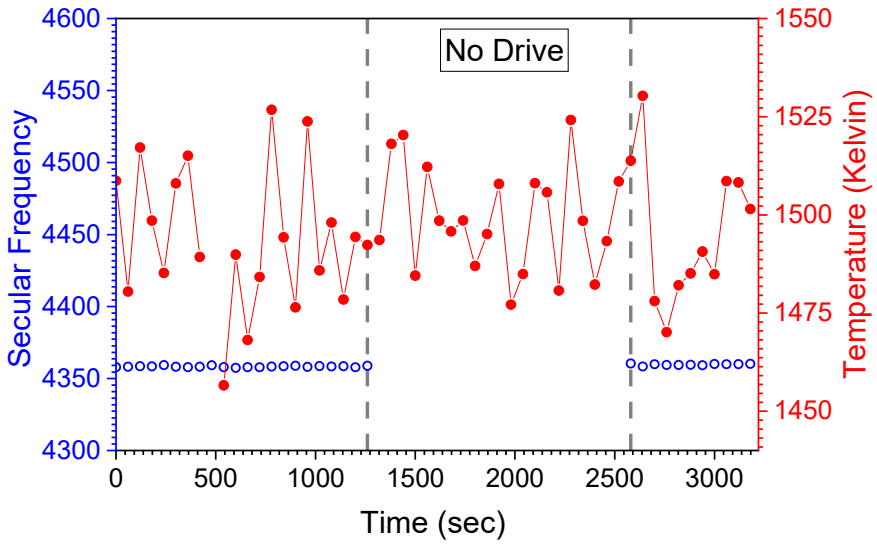

Figure S15. Single Graphite NP with initial mass of 23.22 MDa. In this experiment, the laser was stabilized by using the T_{NP} for slow fluctuations and a PID for fast fluctuations. The drive frequency was turned off between ~1320-2580 seconds showing negligible changes in T_{NP}.

During the first ~1300 seconds, T_{NP} was being measured during the AC drive frequency scan used to measure the secular frequency, hence mass. The extracted T_{NP} was 1500 ± 19 K. At 1320 seconds the AC drive potential was turned off for ~1200 seconds, continuing the spectral measurements. During this

"no drive" time, T_{NP} was 1502 ± 14 K. At 2580 seconds the drive potential was turned back on, and eleven additional simultaneous frequency and T_{NP} measurements were taken, giving T_{NP} = 1498 K ± 19 K. Clearly, any effect of the AC drive potential on the spectra and extracted T_{NP} values is negligible compared to the uncertainty in T_{NP}.

REFERENCES

1. Long, B. A.; Rodriguez, D. J.; Lau, C. Y.; Anderson, S. L., Thermal Emission Spectroscopy for Single Nanoparticle Temperature Measurement: Optical System Design and Calibration. *Appl. Opt.* **2019**, *58*, 642-649.

2. Pon, R. M.; Hessler, J. P., Spectral Emissivity of Tungsten: Analytic Expressions for the 340-Nm to 2.6-Mm Spectral Region. *Appl. Optics* **1984**, *23*, 975-976.

3. De Vos, J. C., A New Determination of the Emissivity of Tungsten Ribbon. *Physica* **1954**, *20*, 690-712.

4. Larrabee, R. D., Spectral Emissivity of Tungsten. *J. Opt. Soc. Am.* **1959**, *49*, 619-625.

5. Marple, D. T. F., Spectral Emissivity of Rhenium. *J. Opt. Soc. Am.* **1956**, *46*, 490-494.

6. Bohren, C. F.; Huffman, D. R., *Absorption and Scattering of Light by Small Particles*; Wiley: New York, 1983.

7. Djurišić, A. B.; Li, E. H., Optical Properties of Graphite. *J. Appl. Phys.* **1999**, *85*, 7404-7410.